JOURNAL OF COMPUTATIONAL PHYSICS **102**, 194–210 (1992)

Implicit Flux Limiting Schemes for Petroleum Reservoir Simulation

MARTIN BLUNT AND BARRY RUBIN

BP Research Centre, Chertsey Road, Sunbury-on-Thames, Middlesex TW16 7LN, United Kingdom

Received April 23, 1990; revised June 20, 1991

Explicit total variation diminishing (TVD) numerical methods have been used in the past to give convergent, high order accurate solutions to hyperbolic conservation equations, such as those governing flow in oil reservoirs. To ensure stability there is a restriction on the size of time step that can be used. Many petroleum reservoir simulation problems have regions of fast flow away from sharp fronts, which means that this time step limitation makes explicit schemes less efficient than the best implicit methods. This work extends the theory of TVD schemes to both fully implicit and partially implicit methods. We use our theoretical results to construct schemes which are stable even for very large time steps. We show how to construct an adaptively implicit scheme which is nearly fully implicit in regions of fast flow, but which may be explicit at sharp fronts which are moving more slowly. In general these schemes are only first-order accurate in time overall, but locally may achieve second-order time accuracy. Results, presented for a one-dimensional Buckley–Leverett problem, demonstrate that these methods are more accurate than conventional implicit algorithms and more efficient than fully explicit methods, for which smaller time steps must be used. The theory is also extended to embrace mixed hyperbolic/parabolic (black oil) systems and example solutions to a radial flow equation are presented. In this case the time step is not limited by the high flow speeds at a small radius, as would be the case for an explicit solution. Moreover, the shock front is resolved more sharply than for a fully implicit method.

1. INTRODUCTION

Explicit flux limiting schemes for the solution of hyperbolic conservation laws have already been discussed in some detail [1, 2]. For one-dimensional scalar equations, it is possible to demonstrate that these schemes are total variation diminishing (TVD), which means that the solutions are stable and will generally converge to the correct physical solution, even if the solution contains discontinuities or shocks. The schemes maintain second-order accuracy in smooth regions and sharply resolve any discontinuities.

In this paper we will construct TVD schemes which are particularly appropriate for solving the component conservation laws in petroleum reservoir simulation, which presents some problems not seen with the solution of the Euler equations. Often in reservoir simulation the pressure field is solved implicitly, followed by an explicit update of the conservation equations, for which high order techniques can be used. In compositional simulation the equilibrium concentration of each hydrocarbon component in gas, oil, and aqueous phases also needs to be calculated at the computed pressures and temperatures in the reservoir. For large multidimensional problems almost all the computer time is spent solving for the fluid pressures and phase equilibrium. The saturation and concentration updates are comparatively fast. However, the use of a low order or unstable numerical technique for updating the saturations can lead to inaccurate results. It is thus generally worthwhile to use a stable high order technique, which improves the resolution of the simulation, without appreciably increasing the total time used. The application of high order Godunov schemes in reservoir simulation has been discussed by Trangenstein *et al.* [3–6]. Another second-order method, flux-corrected transport, has been used in multidimensional fluid flow simulations by Christie and Bond [7]. It is most efficient to solve the pressure equation as infrequently as possible, which implies the use of large time steps. However, the explicit methods which have been proposed may then become unstable. Low order implicit techniques, in contrast, are stable even for large time steps, but the accuracy of the solution is often poor.

There are several circumstances which force the use of implicit schemes even though the accuracy of higher order explicit schemes could be advantageous. These are applications which normally feature very high flows in some restricted region of the reservoir and moderate to low flows elsewhere. Examples include radial flow or quasi-static situations with a front moving slowly perpendicular to a fast flow direction, such as gravity over-ride or coning. In these cases, the regions of high flow drastically reduce the time step possible from explicit formulations, which makes the simulation extremely inefficient. Thus stable implicit methods with a large time step are often used. The implicit models are normally of first-order accuracy in time and space. In the regions of moderate to low flow rates, higher order techniques would greatly improve the accuracy of the model's predictions.

The ideal numerical scheme for reservoir engineering problems would be stable for large time steps and yet

0021-9991/92 $5.00

resolve shock fronts accurately. This can be achieved by an adaptive scheme which is nearly fully implicit in regions of fast flow, but which may be explicit near slower moving shocks. We approach this problem by using methods which have the following properties:

(1) Strictly conservative.

(2) Second-order spatially accurate in smooth regions of the flow.

(3) At best, second-order accurate in time locally.

(4) Unconditionally stable.

We describe several schemes which are appropriate for different types of problems. We discuss:

(1) A second-order space and time-accurate fully explicit TVD scheme due to Sweby [1, 2]. This method has a restriction on the size of time step which can be used. For reservoir engineering problems this approach is suitable for problems where the shock fronts represent the fastest flowing portions of the system, such as the linear Buckley–Leverett problem.

(2) A second-order spatially accurate and first-order time accurate TVD scheme based on scheme (1). This scheme has no particular advantages, but is presented as a building block for an adaptively implicit method.

(3) A fully implicit TVD scheme which is unconditionally stable. This method is ideal for quasi-steady state problems, which feature several regions of fast flow and where the resolution of sharp fronts is not important.

(4) A partially implicit/partially explicit TVD scheme. The degree of implicitness is calculated by a global stability criterion. This scheme is unconditionally stable but allows the accurate resolution of shocks if there are no regions of fast flow. This is a reliable scheme for general purpose simulation.

(5) An adaptively implicit scheme like (4) but based on a local stability criterion, which allows the scheme to be, at best, second-order accurate near slow flowing shocks yet fully implicit and therefore stable in regions of fast flow. This method is appropriate for problems where the fluids are moving rapidly in a region of the reservoir some way from the front, such as radial flow near wells and the gravity override of a light gas over heavier oil or water.

There is some discussion on how the schemes could be extended to two and three dimensions. The schemes we develop have been designed for the simulation of flow in porous media and steady state problems, where it is efficient to use large time steps.

2. CONSTRUCTING NUMERICAL SCHEMES

In this section we will develop TVD schemes for a one-dimensional scalar conservation equation. We will use the theoretical TVD criteria which are derived in the appendix. We begin by constrcuing an explicit method which is, at best, second-order accurate and then consider the temporal stability and accuracy of partially implicit schemes. At the end of this section we will discuss schemes coupled with a parabolic pressure equation.

As a relevant example, we will describe schemes for the solution of the Buckley–Leverett equation. This equation describes the one-dimensional flow of two incompressible fluids ("water" and "oil") in a porous medium. It can be written as

$$\frac{\partial s}{\partial t}+\frac{\partial f}{\partial x}=0, \tag{2.1}$$

where the flux $f(s)$ is a known function of s the saturation of the water phase,

$$f(s)=v_t f_w(s), \tag{2.2}$$

where v_t is the total velocity of the two phase system and the fractional flow of water f_w in the absence of gravity is given by

$$f_w(s)=\frac{K_{rw}(s)/\mu_w}{K_{rw}(s)\,\mu_w+K_{ro}(s)/\mu_o}; \tag{2.3}$$

K_{rw} and K_{ro} are the relative permeabilities of the water and oil phases, respectively, and μ_w and μ_o are the fluid viscosities.

2.1. Explicit Flux Limited Schemes

In this section we will briefly review explicit TVD schemes before constructing novel implicit methods. We will develop flux limiting schemes following the approach of Sweby [1, 2]. These schemes have also been described by van Leer, and Roe, Sweby and Baines, [8–12]. Other explicit high order methods include Godunov schemes [13], which have been applied to black oil models [3–6], and flux corrected transport [14], which has been extended to multidimensional, multicomponent fluid flows [7].

First-order schemes, such as the Engquist–Osher method [15] are stable and convergent and obey the TVD criteria derived in the appendix. However, numerical dispersion smears out the shock fronts, so the solutions are only accurate if a large number of grid blocks are used. Most unconstrained second-order schemes such as Lax–Wendroff and two-point upstream weighting suffer from less numerical dispersion, but produce spurious oscillations about shock fronts.

Flux limiting methods are both accurate and stable. Thus discontinuities are resolved accurately without either excessive smearing or unphysical oscillatory instabilities.

This is achieved by limiting the second-order corrections to the numerical flux to obey the TVD criteria. If this is done the total variation in the solution will not increase with time: a monotonic profile (no maxima or minima) will remain monotonic without developing unstable and unphysical blips.

We write an explicit finite difference approximation to the saturation update as

$$s_i^{n+1} = s_i^n - \lambda[F_{i+1/2}^n - F_{i-1/2}^n]. \tag{2.4}$$

The superscripts and subscripts refer to the time step and the grid block respectively. $\lambda = \Delta t/\Delta x$. $F_{i+1/2}$ and $F_{i-1/2}$ represent numerical approximations to the flux, f, across the grid cell edges. If we assume that the characteristic velocity of the saturation profile, $v = df/ds$, is positive, then we find an approximation for F about an upstream value F_i^n, which is accurate to second order in space and time (i.e., up to $O(\Delta x)^2$, $O(\Delta t)^2$):

$$F_{i+1/2}^n = F_i^n + \frac{\phi_{i+1/2}^n}{2}(F_{i+1}^n - F_i^n)(1 - \lambda v_i^n). \tag{2.5}$$

F_i^n represents the flux f calculated at s_i^n and $v_i^n = df/ds|_{s=s_i^n}$. The first term in (2.5) gives single point upstream weighting. The second terms are $O(\Delta x)^2$, $O(\Delta t)^2$ corrections to the numerical fluxes. ϕ, the limiter, is a function of r, which is a ratio of successive second-order terms,

$$r_{i+1/2}^n = \frac{(F_i^n - F_{i-1}^n)(1 - \lambda v_{i-1}^n)}{(F_{i+1}^n - F_i^n)(1 - \lambda v_i^n)} \tag{2.6}$$

and $\phi(r_{i+1/2}^n)$ is written as $\phi_{i+1/2}^n$ in (2.5).

The results of the appendix may be used to find limits on the function $\phi(r)$ such that the scheme remains TVD. Since this section is a review of previous work, we will not derive these limits here. Derivations of the TVD region are given in Ref. [1] and are also demonstrated in Section 2.3 as a special case of a partially implicit method. We would also like the scheme to be second-order accurate in smooth, monotonic portions of the profile. Figure 1 shows the second-order and TVD regions of the function $\phi(r)$. A suitable choice of function, which gives good results is the van Leer limiter [9]

$$\phi = \frac{r + |r|}{1 + r}. \tag{2.7}$$

It is worth pointing out that when $\phi = 0$ the scheme reverts to single-point upstream, which is only first-order accurate. When $\phi = r$, we have the Beam–Warming scheme. When $\phi = 1.0$, the scheme is Lax–Wendroff and, when $\phi = 2.0$, the scheme uses a downstream weighted flux. All of these values of ϕ are possible when the van Leer limiter is used.

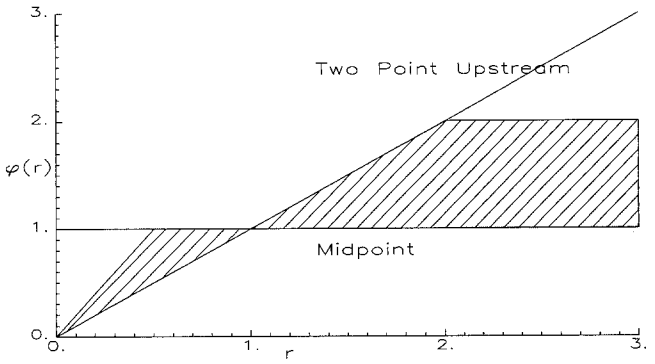

FIG. 1. Second-order TVD region. The second-order TVD region is shaded. The limiters corresponding to the midpoint and two-point upstream schemes are indicated.

The maximum time step that can be used before the method becomes unstable (the TVD criteria are violated) is dependent on the Courant–Friedrichs–Lewy (CFL) condition [16]. If $v_{\max}$ is the largest wavespeed (df/ds) encountered, then the CFL number is defined as $\lambda v_{\max}$. The van Leer limiter is stable for CFL numbers $\leqslant 1$.

Figure 2 compares this TVD scheme with the single-point upstream scheme (all explicit) for a non-linear waterflood, using the flux function

$$f(s) = \frac{3s^2}{3s^2 + (1-s)^2} \tag{2.8}$$

and a CFL number of 0.4. The exact solution (shown by the solid curve) has a shock front from a saturation of 0.5 to zero. The single point upwind scheme ($\phi = 0$) smears this front over several grid blocks. The TVD method decreases

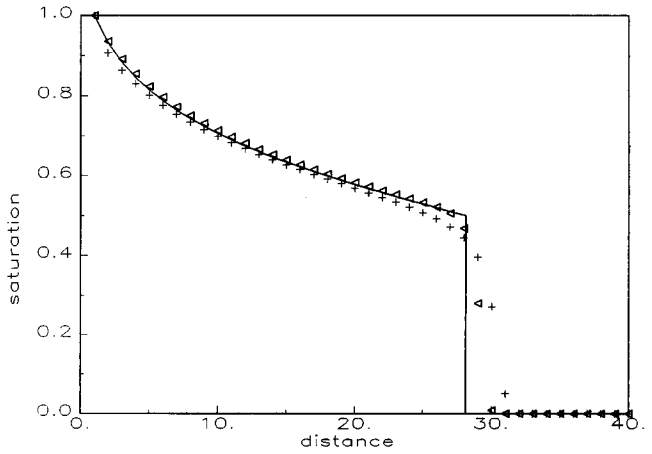

FIG. 2. Solutions to a Buckley–Leverett problem with explicit schemes and a CFL number of 0.4 and $N = 40$ grid blocks. Crosses, first-order upstream; triangles, flux-limiting method. The solid line is the exact solution.

the numerical diffusion and resolves the discontinuity over approximately half the grid blocks required by the first-order method.

2.1.1. *First-Order Explicit Scheme*

A simplified version of this TVD scheme, which is second-order spatially accurate, but only first-order accurate in time, writes the cell edge flux $F_{i+1/2}$ as

$$F^n_{i+1/2} = F^n_i + \frac{\phi^n_{i+1/2}}{2}(F^n_{i+1} - F^n_i), \tag{2.9}$$

where the time correction $(1-\lambda v^n_i)$ has been ignored. The scheme is the same as before, where we define

$$r^n_{i+1/2} = \frac{F^n_i - F^n_{i-1}}{F^n_{i+1} - F^n_i} \tag{2.10}$$

and use the van Leer limiter, (2.7). When $\phi = r$, the scheme is the two-point upstream weighted scheme. When $\phi = 1.0$, the scheme is midpoint weighted and when $\phi = 2.0$, the scheme uses a downstream weighted flux. On its own there is nothing to recommend this scheme as it is only $O(\Delta t)$ and only stable for CFL numbers up to $\frac{1}{2}$, rather than 1 for the second-order method. We only introduce the scheme here, since it will be used to construct a partially implicit, partially explicit method which reintroduces a second-order time correction to the flux. The advantage is that then stable solutions can still be calculated, even for CFL numbers greater than 1.

Figure 3 compares this method with single-point upstream weighting for the example problem shown in Fig. 2.

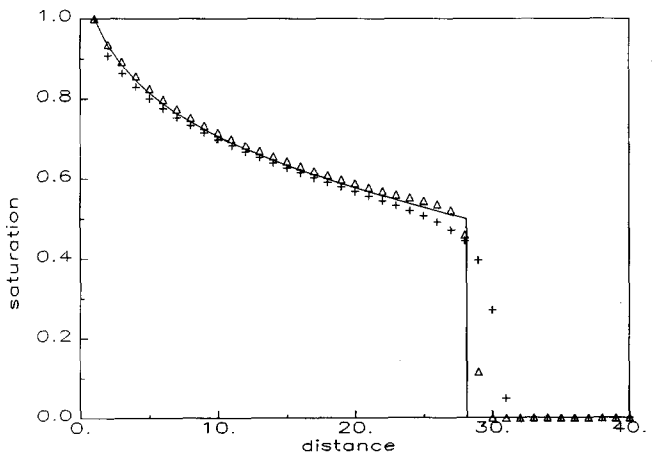

FIG. 3. Solutions to a Buckley–Leverett problem as in Fig. 2. Crosses, first-order upstream weighting; triangles, a simplified first-order in time flux limiting scheme.

2.1.2. *Error Norms*

We may quantify the accuracy of the schemes by computing error norms. An l norm L_l is defined as

$$L_l = \left(\sum_{i=1}^{N} \frac{1}{N} |s_i - s_i^{\text{exact}}|^l \right)^{1/l}, \tag{2.11}$$

where s_i^{exact} is the exact solution at the centre of grid block i in a computation over N cells. L_l is calculated on grids of various N at a fixed value of λ. The order p of the scheme is defined such that as $N \to \infty$, $L_l \sim N^{-p}$. For exact solutions which feature a discontinuity, such as the Buckley–Leverett problem presented here, the error is dominated by $O(1)$ inaccuracies in the few computed points near the shock, where even a flux limited scheme reverts to first order to ensure stability. Thus, at best we expect $L_1 \approx C/N$ for large N and some finite prefactor, C. C will depend on the problem and the scheme.

Figure 4 shows N times the L_1 norm plotted against $\log N$. For first-order convergence NL_1 is a constant, C. Single point upstream weighting appears, for this problem, to display worse than $O(1/N)$ convergence. The simplified TVD method is a considerable improvement over single-point upstream weighting, although it is not as good as the Sweby TVD method.

The flux limited scheme with a time correction is "second order" in the sense that we do see $O(N^{-2})$ convergence of the error norms for problems whose exact solutions are continuous with continuous first derivatives [17]. This may be demonstrated by looking at a simpler problem—the linear

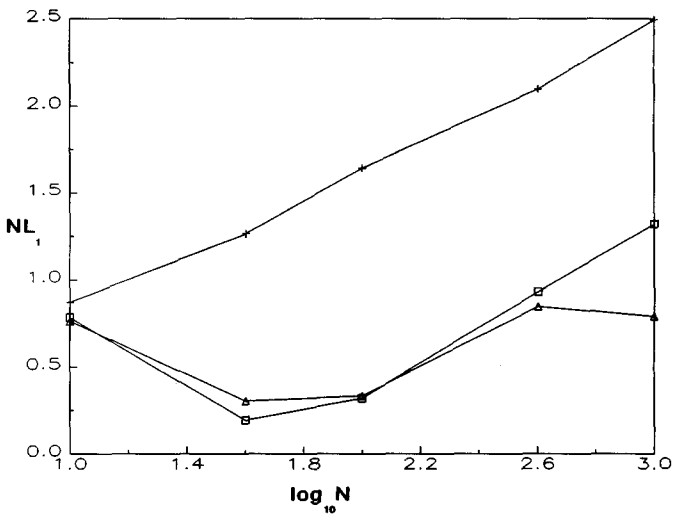

FIG. 4. L_1 error norm multiplied by the number of grid blocks N as a function of $\log_{10} N$. Crosses, single-point upstream weighting; triangles, Sweby flux limiting scheme; squares, time-uncorrected flux limiter. The error norm is computed on the solution to the Buckley–Leverett problem. The presence of the shock means that at best the schemes are first-order convergent—NL_1 is a constant.

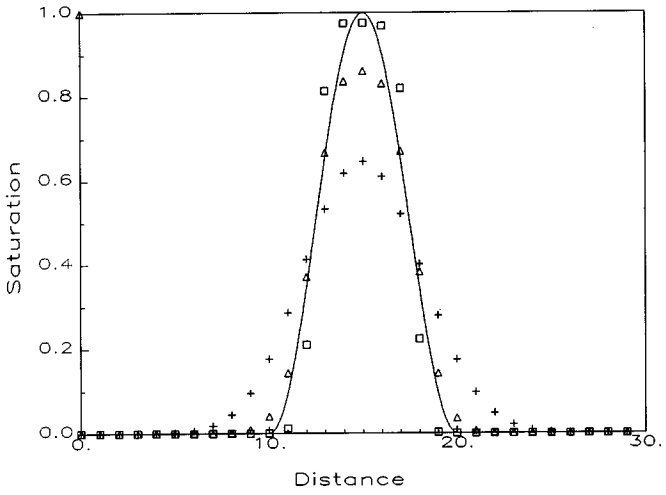

FIG. 5. Linear convection of a $\sin^2$ pulse at a CFL number of 0.4 across one-third of the grid with $N=30$. Crosses, single-point upstream weighting; triangles, Sweby flux limiting scheme; squares, time-uncorrected flux limiter.

advection of a pulse. We set the flux $f(s)=s$ and use an initial condition $s(x, 0)=\sin^2(3\pi(x-1)/N)$ for $N/3 \geqslant x \geqslant 0$ and $s(x, 0)=0$ elsewhere. We set $\Delta x=1$. Figure 5 shows the computed and exact profiles after transport across one-third of the grid at a CFL number of 0.4 with $N=30$. The flux–limiting scheme without time correction tends to over-square the profile. Figure 6 shows the L_1 error norms for $N=30$ to $N=3000$. The Sweby TVD scheme displays second-order accuracy, while the single-point upstream weighted scheme and the simple flux limiter are only first-order accurate.

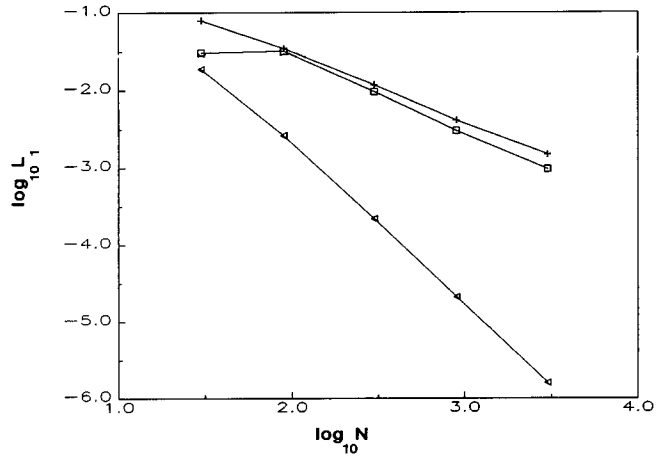

FIG. 6. L_1 error norms; $\log_{10} L_1$ is plotted against $\log_{10} N$ for the linear advection problem shown in Fig. 5. Crosses, single-point upstream weighting; triangles, Sweby flux limiting scheme; squares, time-uncorrected flux limiter.

2.2. Implicit Methods

Based on the explicit scheme described in Section 2.1.1, an implicit version of the TVD midpoint scheme will now be developed. Implicit modelling requires the calculation and use of fluxes and limiters at the unknown $(n+1)$th time level.

Following from the previous section the scheme is set up as

$$s_i^{n+1}-s_i^n+\lambda[F_{i+1/2}^{n+1}-F_{i-1/2}^{n+1}]=0. \tag{2.12}$$

As before, if df/ds is positive, an approximation for F is

$$F_{i+1/2}^{n+1}=F_i^{n+1}+\frac{\phi_{i+1/2}^{n+1}}{2}(F_{i+1}^{n+1}-F_i^{n+1}). \tag{2.13}$$

F_i^{n+1} represents the flux f calculated at s_i^{n+1}; ϕ, the limiter, is function of r, where r is now calculated at the $(n+1)$th time level,

$$r_{i+1/2}^{n+1}=\frac{F_i^{n+1}-F_{i-1}^{n+1}}{F_{i+1}^{n+1}-F_i^{n+1}}. \tag{2.14}$$

As above we choose the van Leer limiter, (2.7).

2.2.1. *Solution by Newton-Raphson Iteration*

Equation (2.12) is a non-linear expression for s_i^{n+1}, which can be solved using Newton–Raphson iteration [18, 19]. Equation (2.12) may be written as

$$G(s_i^{n+1})=0, \tag{2.15}$$

where

$$G(s_i^{n+1})=s_i^{n+1}-s_i^n+\lambda[F_{i+1/2}^{n+1}-F_{i-1/2}^{n+1}] \tag{2.16}$$

and s_i^n is known, and the numerical fluxes, F, as functions of s_i^{n+1} may be calculated as above. The solution is obtained iteratively. For the first iteration $(k=1)$ we use $s_i^{k=1}=s_i^n$. Subsequent estimates for the updated saturations are found as follows. First, we define the difference in saturation between two Newton iterations:

$$\delta s_i=s_i^{k+1}-s_i^k. \tag{2.17}$$

We assume that s_i^k is known and we calculate δs to find a more accurate estimate of s_i^{n+1}. Then to first order in the small quantity δs,

$$G_i^{k+1}=G_i^k+\left(\frac{\partial G_i}{\partial s_j}\right)^k \delta s_j, \tag{2.18}$$

where the superscript on G labels the iteration and the subscript labels the grid block. The value of δs_j which makes $G_i^{k+1} = 0$, (2.15), obeys the expression

$$\left(\frac{\partial G_i}{\partial s_j}\right)^k \delta s_j = -G_i^k. \tag{2.19}$$

$\partial G_i/\partial s_j$ is a matrix of derivatives, which must be inverted to calculate δs in (2.19). For a first-order scheme, G_i is a function only of the saturations in the cells i and $i-1$, and hence the derivative matrix (Jacobian) has a simple lower triangular form. However, in the more sophisticated high order schemes considered here, the Jacobian may have many non-zero elements, which makes the matrix inversion difficult. For this reason we simplify our treatment and consider only first-order terms in the calculation of $\partial G_i/\partial s_j$. The quantity $-G_i^k$ on the right-hand side of (2.19) is still calculated to second order, and hence we converge to the correct high order solution.

The non-zero terms in the Jacobian are then as follows:

$$\left(\frac{\partial G_i}{\partial s_i}\right)^k = 1 + \lambda \left.\frac{df(s)}{ds}\right|_{s=s_i^k} \tag{2.20}$$

and

$$\left(\frac{\partial G_i}{\partial s_{i-1}}\right)^k = -\lambda \left.\frac{df(s)}{ds}\right|_{s=s_{i-1}^k}. \tag{2.21}$$

The iteration continues until the calculated δs_j in (2.19) is smaller than some convergence criterion. In the examples we present, we calculated the maximum δs_j over all the grid blocks and compared it with the L_1 and L_∞ error norms. If this was less than $0.1L_1$ and $0.1L_\infty$, the iteration was stopped. This ensured that the dominant error came from the inadequacies of the scheme rather than failure of the Newton–Raphson iteration to converge. The efficiency of any implicit algorithm is limited by the number of iterations necessary to produce convergence.

2.2.2. *Results*

In the next section we will show that this scheme is stable for all CFL numbers. Figures 7 and 8 show results from implicit schemes, for the flux function given by (2.8). Figure 7 shows results using a single-point upstream weighted implicit flux at CFL numbers of 0.4, 1, and 4, which required on average 3, 3, and 5 Newton iterations per time step, respectively. Note that the single-point upstream implicit scheme is more diffusive than its explicit counterpart (Fig. 2) at the same CFL number. For CFL numbers greater than 1, outside the explicit stability limit, the shock front is very poorly resolved.

Figure 8 shows solutions using a TVD flux limiter at CFL numbers of 0.4, 1, and 4 which needed on average 3, 4, and 6 Newton iterations per time step, respectively, to ensure convergence. The results are superior to single-point upstream weighting. The shock front is still more diffuse at a CFL number of 0.4, compared with an explicit method (Fig. 2 or 3), but the scheme is stable for larger time steps. Figure 9 shows the L_1 error norm at a CFL number of 0.4. The single-point implicit scheme, like its explicit analogue shows worse than $1/N$ convergence, whilst the TVD scheme gives superior results and appears to be strictly first-order accurate as $N \to \infty$.

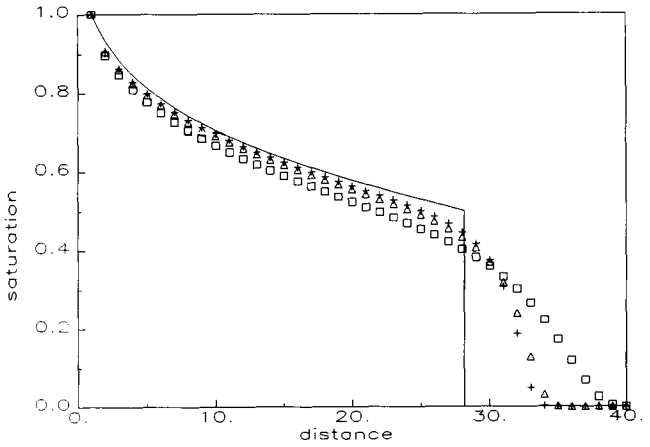

FIG. 7. Solutions with a first-order implicit scheme with $N = 40$. Squares, CFL number of 4; triangles, CFL = 1; crosses, CFL = 0.4.

Yee *et al.* have proposed TVD implicit schemes [20–22], but found that convergence to the correct solution by Newton iteration using the full Jacobian was very slow if a high order limited implicit flux was used. They suggested a linearized non-conservative TVD implicit scheme. The number of extra Newton iterations required for convergence with a high order method in the example above, however,

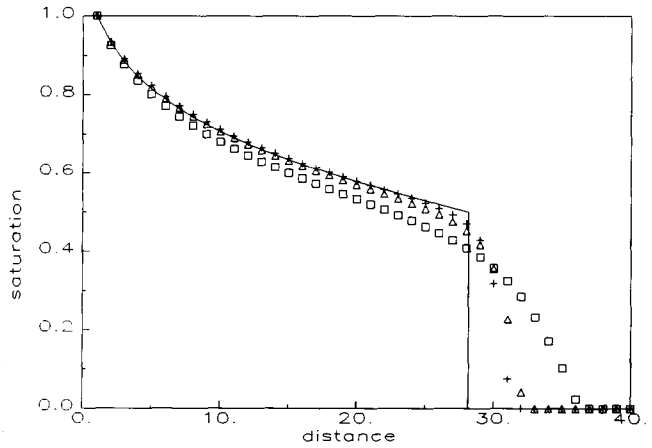

FIG. 8. Solutions with a flux limited implicit TVD scheme with $N = 40$. Squares, CFL number of 4; triangles, CFL = 1; crosses, CFL = 0.4.

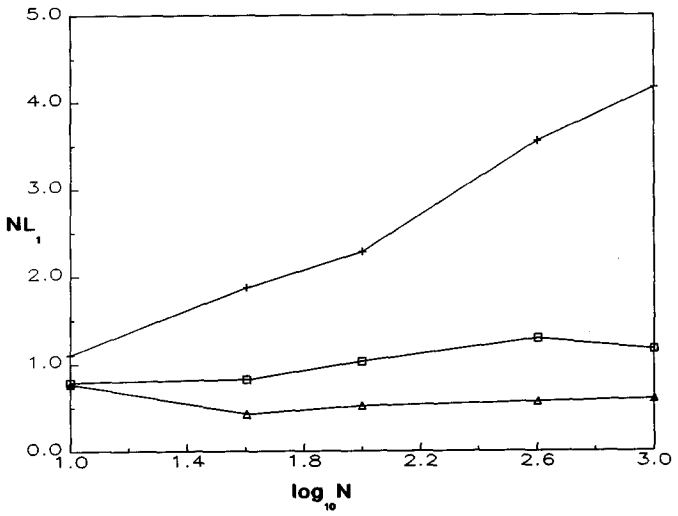

FIG. 9. L_1 error norm multiplied by the number of grid blocks N as a function of $\log_{10} N$ as in Fig. 4. Crosses, implicit single-point upstream weighting; triangles, partially implicit flux-limiting scheme with $\theta = \frac{1}{2}$; squares, fully implicit flux limiter.

was small using a first-order Jacobian and was more than compensated by the improved accuracy of the solution.

In the examples below, a low order Jacobian is always used, and the number of iterations needed for convergence only ever exceeds a fully first-order method by one or two.

2.3. TVD Schemes with Temporal Weighting

We will now write down a conservative equation for the saturation update, which is partially implicit. In the previous section we described a scheme which was first-order accurate in time, but stable for large time steps. In this section we will use a partially implicit method, which gives improved time accuracy without the CFL constraint seen in totally explicit schemes. The form of the update is

$$s_i^{n+1} - s_i^n = -\lambda[(1-\theta_{i+1/2})\, F^n_{i+1/2} - (1-\theta_{i-1/2})\, F^n_{i-1/2}] - \lambda[\theta_{i+1/2} F^{n+1}_{i+1/2} - \theta_{i-1/2} F^{n+1}_{i-1/2}]. \quad (2.22)$$

We will attempt to construct a scheme where θ, the degree of implicitness, is fixed by a local stability constraint. The time step should be chosen so that the scheme sharply resolves shock fronts by being second-order accurate, while remaining stable in regions of great throughput, where θ approaches 1. The scope of this method is similar to the work of Fryxell *et al.* [23], who applied an adaptively implicit–explicit high order Godunov scheme to Lagrangian hydrodynamics.

TVD schemes based on (2.22) have been studied by Yee *et al.* [20, 22]. However, as mentioned above they solved a linearized form of this equation and only considered a fixed value of θ. Our work will be conservative, at best second-order spatially accurate for both explicit and implicit fluxes, and we will also allow the values of θ to be different for different cell edges.

The parameters $\theta_{i+1/2}$ and $\theta_{i-1/2}$ give the degree of implicit weighting in the numerical flux across the right- and left-hand edges of cell i, respectively. $\theta = 1$ represents a fully implicit scheme, (2.12), while $\theta = 0$ is explicit, (2.4).

The non-linear equation (2.22) is solved iteratively by the Newton–Raphson technique, as described in Section 2.2.1, except that now $G(s_i^{n+1})$ is given by

$$G(s_i^{n+1}) = s_i^{n+1} - s_i^n + \lambda[(1-\theta_{i+1/2})\, F^n_{i+1/2} - (1-\theta_{i-1/2})\, F^n_{i-1/2}] + \lambda[\theta_{i+1/2} F^{n+1}_{i+1/2} - \theta_{i-1/2} F^{n+1}_{i-1/2}]. \quad (2.23)$$

As in the previous sections, we find an approximation for $F^n_{i+1/2}$ using Eq. (2.5). $F^{n+1}_{i+1/2}$ is calculated from (2.13). The limiter ϕ is chosen to make the spatial approximation in (2.22) both accurate and TVD. The weighting θ controls the temporal accuracy of the solution: $\theta = \frac{1}{2}$ gives a scheme which is second order in time, while a fully implicit method, with $\theta = 1$, is stable for all λ. We will show later how we control θ to give us a stable solution of the greatest possible accuracy. Writing out (2.22) in full and rearranging terms gives

$$\begin{aligned} s_i^{n+1} - s_i^n = &-\lambda(\theta_{i+1/2} - \theta_{i-1/2})(F_i^{n+1} - F_i^n) \\ &-\lambda(1-\theta_{i-1/2})(F_i^n - F_{i-1}^n) \\ &-\lambda\theta_{i-1/2}(F_i^{n+1} - F_{i-1}^{n+1}) \\ &-\frac{\lambda\phi^n_{i+1/2}}{2}(1-\theta_{i+1/2})(F^n_{i+1} - F^n_i) \\ &+\frac{\lambda\phi^n_{i-1/2}}{2}(1-\theta_{i-1/2})(F^n_i - F^n_{i-1}) \\ &-\frac{\lambda\phi^{n+1}_{i+1/2}}{2}\theta_{i+1/2}(F^{n+1}_{i+1} - F^{n+1}_i) \\ &+\frac{\lambda\phi^{n+1}_{i-1/2}}{2}\theta_{i-1/2}(F^{n+1}_i - F^{n+1}_{i-1}). \end{aligned} \quad (2.24)$$

We now define the following quantities: a ratio of successive flux differences, $r^n_{i+1/2}$, which is given by (2.10), and effective velocities or flux gradients, defined by a spatial derivative,

$$v_i^n = \frac{F_i^n - F_{i-1}^n}{s_i^n - s_{i-1}^n}, \quad (2.25)$$

and a temporal derivative,

$$u_i^n = \frac{F_i^{n+1} - F_i^n}{s_i^{n+1} - s_i^n}. \quad (2.26)$$

Equation (2.24) yields

$$[1+\lambda u_i^n(\theta_{i+1/2}-\theta_{i-1/2})](s_i^{n+1}-s_i^n)$$
$$=-\lambda v_i^n\,\Delta s_{i-1}^n\left[(1-\theta_{i-1/2})\left(1-\frac{\phi_{i-1/2}^n}{2}\right)+(1-\theta_{i+1/2})\frac{\phi_{i+1/2}^n}{2r_{i+1/2}^n}\right]-\lambda v_i^{n+1}\,\Delta s_{i-1}^{n+1}$$
$$\times\left[\theta_{i-1/2}\left(1-\frac{\phi_{i-1/2}^{n+1}}{2}\right)+\theta_{i+1/2}\frac{\phi_{i+1/2}^{n+1}}{2r_{i+1/2}^{n+1}}\right]. \tag{2.27}$$

We now compare this equation with (A1) of the Appendix. We can see that the coefficients D^{n+1} and D^n are zero, which is consistent with a TVD scheme, (A8). The TVD criteria for the coefficients C give us, for C^{n+1},

$$\frac{\lambda v_i^{n+1}\left[\theta_{i-1/2}\left(1-\frac{\phi_{i-1/2}^{n+1}}{2}\right)+\theta_{i+1/2}\frac{\phi_{i+1/2}^{n+1}}{2r_{i+1/2}^{n+1}}\right]}{1+\lambda u_i^n(\theta_{i+1/2}-\theta_{i-1/2})}\geqslant 0 \tag{2.28}$$

and, for C^n,

$$1+\lambda u_i^n(\theta_{i+1/2}-\theta_{i-1/2})\geqslant\lambda v_i^n\left[(1-\theta_{i-1/2})\left(1-\frac{\phi_{i-1/2}^n}{2}\right)+(1-\theta_{i+1/2})\frac{\phi_{i+1/2}^n}{2r_{i+1/2}^n}\right]\geqslant 0. \tag{2.29}$$

From (2.29) it can be seen that the denominator in (2.28) must be positive and so we are left with a simpler relation,

$$\lambda v_i^{n+1}\left[\theta_{i-1/2}\left(1-\frac{\phi_{i-1/2}^{n+1}}{2}\right)+\theta_{i+1/2}\frac{\phi_{i+1/2}^{n+1}}{2r_{i+1/2}^{n+1}}\right]\geqslant 0. \tag{2.30}$$

Equations (2.29) and (2.30) are the major theoretical results of this paper. A scheme which conforms to the constraints above for all grid blocks i will be TVD.

2.3.1. *Explicit Schemes*

A partially implicit scheme will have values of θ in the region $0\leqslant\theta\leqslant 1$. For an explicit scheme, $\theta_{i+1/2}=0$ in all grid blocks i. Equation (2.30) reduces trivially to $0\geqslant 0$, but (2.29) gives the following restriction:

$$1\geqslant\lambda v_i^n\left(1-\frac{\phi_{i-1/2}^n}{2}+\frac{\phi_{i+1/2}^n}{2r_{i+1/2}}\right)\geqslant 0; \tag{2.31}$$

λv_i^n is always chosen to be positive. This expression must be obeyed for all choices of $\phi_{i+1/2}$ and $\phi_{i-1/2}$. If we require that

$$2\geqslant\phi(r)\geqslant 0 \tag{2.32}$$

and

$$2\geqslant\frac{\phi(r)}{r}\geqslant 0, \tag{2.33}$$

then (2.31) is obeyed subject to the stability limit $\lambda v_i^n\leqslant\frac{1}{2}$. If this holds everywhere, the CFL number must be less than $\frac{1}{2}$. We mentioned this condition in Section 2.1.1. The TVD region described by Eqs. (2.32) and (2.33) is illustrated graphically in Fig. 1.

2.3.2. *Implicit Schemes*

Here $\theta_{i+1/2}=\theta_{i-1/2}=1$. In this case it is (2.29) which reduces to a trivial expression. From (2.30) we find:

$$\lambda v_i^{n+1}\left(1-\frac{\phi_{i-1/2}}{2}+\frac{\phi_{i+1/2}}{2r_{i+1/2}}\right)\geqslant 0. \tag{2.34}$$

If we use the same constraints on the function ϕ as in Eqs. (2.32) and (2.33), then (2.34) is satisfied for all CFL numbers. If the limiter is TVD, there is no restriction on the size of time step.

2.3.3. *Partially Implicit Cases*

The motivation behind a partially implicit scheme is now clear. For intermediate values of θ we will be allowed to use larger time steps than for an explicit scheme, while retaining the improved resolution of shock fronts which is characteristic of explicit TVD methods. Moreover, if $\theta=\frac{1}{2}$ the scheme is second-order accurate in time. Our scheme will be TVD if (2.29) and (2.30) are obeyed.

We can simplify our analysis by keeping the constraints on ϕ, (2.32), and (2.33) which we used for totally implicit and totally explicit methods. Then (2.29) and (2.30) are both obeyed (bar a restriction on the maximum CFL number) if $1+\lambda u_i^n(\theta_{i+1/2}-\theta_{i-1/2})\geqslant 0$ and the velocities v_i^n and v_i^{n+1} are positive. v_i^n and v_i^{n+1} should be positive if we choose to upstream weight our approximation for F. A discussion of a suitable scheme where v changes sign between two grid blocks or time steps is given below.

For a given time step we need to find values of θ sufficiently close to 1 to ensure stability. Schemes which choose different values of θ to obey the inequalities above will have different stability limits. In the next section we propose several different methods, all of which are TVD, and which we test by finding numerical solutions to the Buckley–Leverett equation.

2.3.4. *Flow Reversal and Sonic Points*

In this discussion we have always assumed that there is an unambiguous definition of the direction of the flow, which does not change sign over a single grid block or during a

time step. Imagine that we attempt to calculate the numerical fluxes $F^n_{i+1/2}$ and $F^{n+1}_{i+1/2}$. If v^n_i, v^n_{i+1}, v^{n+1}_i, and v^{n+1}_{i+1} are not all of the same sign, then the upstream direction is ambiguous, and a first-order Engquist–Osher flux must be used [15]. This is defined as

$$F^n_{i+1/2} = F^n_i + \int_{s^n_i}^{s^n_{i+1}} \min\left(\frac{\partial f}{\partial s}, 0\right) ds \tag{2.35}$$

and for the $(n+1)$th time level:

$$F^{n+1}_{i+1/2} = F^{n+1}_i + \int_{s^{n+1}_i}^{s^{n+1}_{i+1}} \min\left(\frac{\partial f}{\partial s}, 0\right) ds. \tag{2.36}$$

These expressions reduce to the familiar upstream weighted fluxes unless df/ds changes sign in the integrand (there is a sonic point). If df/ds is positive in both integrals then the upstream direction is well defined and second-order corrections to the flux may be calculated as described above. If df/ds is negative then $F^n_{i+1/2} = F^n_{i+1}$ and similarly for the $(n+1)$th time level. The second-order fluxes are calculated as before except that the subscript i is replaced by $i+1$ and $i-1$ by i.

If s_i and s_{i+1} straddle a sonic point then both (2.35) and (2.36) reduce to

$$F_{i+1/2} = f_{\min}, \tag{2.37}$$

where $f_{\min}$ is the minimum value of f, i.e., its value where $v = df/ds = 0$. If f is known analytically, f_{min} may be calculated exactly. Where this is not the case, a quadrature rule, using

and

$$v_w = -\frac{KK_{rw}\rho_w}{\mu_w}\frac{\partial p}{\partial x}, \tag{2.39}$$

where we have ignored capillary pressure. K is the absolute permeability, K_r is the relative permeability, ρ is the phase density, μ is the viscosity, and p is the pressure. We then define a total flow $v_t = v_o + v_w$, where

$$v_t = -M\frac{\partial p}{\partial x}. \tag{2.40}$$

M is the total mobility:

$$M = K\left(\frac{K_{ro}\rho_o}{\mu_o} + \frac{K_{rw}\rho_w}{\mu_w}\right). \tag{2.41}$$

The conserved quantities are now no longer the saturations, but the mass of each phase, $m = \Phi\rho s$. This leads to two hyperbolic equations for the phase masses,

$$\frac{\partial m_o}{\partial t} + \frac{\partial}{\partial x}(v_t f_o) = 0 \tag{2.42}$$

for oil and

$$\frac{\partial m_w}{\partial t} + \frac{\partial}{\partial x}(v_t f_w) = 0 \tag{2.43}$$

for water. f_o and f_w are the fractional flow of oil and water

The pressure equation is derived from a pore volume constraint: the sum of the oil and water saturations $s_t = s_o + s_w = 1$. The value of s_t after one saturation update may be slightly different from 1. The error in s_t over Δt is fed in as a source term, so that

$$\frac{ds_t}{dt} = 0 = \frac{1 - s_t}{\Delta t}$$

$$= \frac{\partial s_t}{\partial p}\frac{\partial p}{\partial t} + \frac{\partial s_t}{\partial m_o}\frac{\partial m_o}{\partial t} + \frac{\partial s_t}{\partial m_w}\frac{\partial m_w}{\partial t}. \tag{2.45}$$

In Section 3.4 we describe how we solve this parabolic pressure equation for slightly compressible two phase flow.

3. PRACTICAL IMPLEMENTATION

In the previous section we developed the theory of high order flux limiting schemes to include partially implicit methods. One special case, which had been studied previously, was an explicit scheme, for which we derived TVD criteria for the flux limiter ϕ. If the same limiter was used for a totally implicit formulation, then we arrived at a spatially second-order accurate method which was stable for all finite CFL numbers.

We propose to use the same spatial flux limiter for our partially implicit schemes. However, this still leaves the choice of θ, the Crank–Nicholson weighting parameter undetermined. In this section we discuss several possible choices for θ, derive the stability limits for the proposed schemes, and present example numerical results.

First, we give results for a Buckley–Leverett problem. Then the advantages of a partially implicit scheme are demonstrated by a radial flow example. Last, results from a one-dimensional compressible flow model with coupled pressure and saturation equations are presented.

3.1. A Fixed Implicit Weighting

The analysis of the previous section allowed for a weighting θ which could change from one grid cell edge to the next. We could simplify the equations considerably by having a fixed θ, which would be determined by a global stability constraint. We will assume that θ lies in the range $1 \geqslant \theta \geqslant 0$.

We start from (2.30) with $\theta_{i+1/2} = \theta_{i-1/2} = \theta$, from which we obtain

$$\lambda v_i^{n+1}\theta\left(1 - \frac{\phi_{i-1/2}^{n+1}}{2} + \frac{\phi_{i+1/2}^{n+1}}{2r_{i+1/2}^{n+1}}\right) \geqslant 0 \tag{3.1}$$

and (2.29) gives a similar condition,

$$1 \geqslant \lambda v_i^n(1-\theta)\left(1 - \frac{\phi_{i-1/2}^{n}}{2} + \frac{\phi_{i+1/2}^{n}}{2r_{i+1/2}^{n}}\right) \geqslant 0. \tag{3.2}$$

Equation (3.1) and the right-hand limit of (3.2) are always obeyed for $1 \geqslant \theta \geqslant 0$. To find the global restriction on θ we consider the most constraining values of $\phi_{i-1/2}$, $\phi_{i+1/2}$, and v_i^n in (3.2). These are: $\phi_{i-1/2} = 0$, $\phi_{i+1/2}/r_{i+1/2} = 2$, and $v_i^n = v_{\max}$. The left-hand limit in (3.2) then becomes

$$\lambda v_{\max}(1-\theta) \leqslant \tfrac{1}{2}. \tag{3.3}$$

Equation (3.3) can be used to find the values of θ for which a scheme at a given CFL number will be stable.

If $\theta = \frac{1}{2}$, the scheme is second-order accurate in time, but for large CFL numbers a value of θ closer to 1 must be chosen to maintain the TVD property. A natural choice of scheme is one where θ is chosen to be as close to $\frac{1}{2}$ as possible; i.e.,

$$\theta = \max\left[\frac{1}{2}, 1 - \frac{1}{2\lambda v_{\max}}\right]. \tag{3.4}$$

Note that this method maintains second-order accuracy for CFL numbers less than 1. The TVD scheme described in Section 2.1 was also second-order time accurate and stable up to CFL numbers of 1 [1]. The advantage with this partially implicit method is that larger time steps may be automatically accommodated.

3.1.1. *Results*

Numerical solutions to the Buckley–Leverett equation are shown in Fig. 10 at CFL numbers of 0.4, 1, and 4. The number of Newton iterations per timestep were 3, 3, and 5, respectively, which is similar to the cases illustrated in Fig. 8. For the solutions with CFL numbers less than or equal to 1, $\theta = \frac{1}{2}$ and the scheme is second-order accurate in

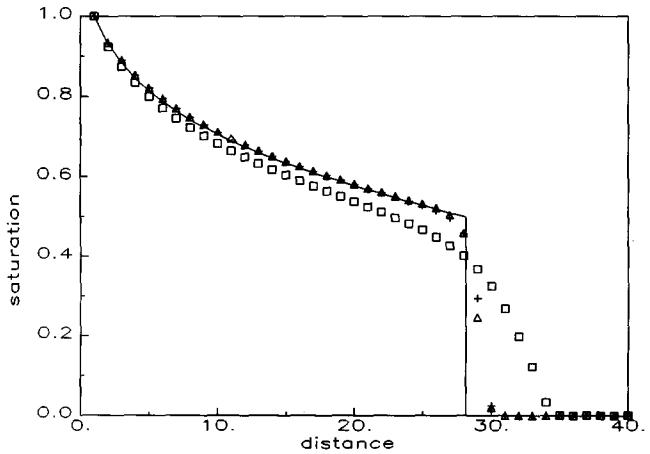

FIG. 10. Solutions with a TVD partially implicit scheme with a fixed value of θ and $N = 40$. Squares, CFL number of 4; triangles, CFL = 1; crosses, CFL = 0.4.

both space and time. The resolution of the shock front is comparable with that for the explicit TVD scheme shown in Fig. 2. For a CFL number of 4, $\theta = \frac{7}{8}$ from (3.4). Although the shock is now smeared over several grid blocks, the solution is as accurate as a first-order implicit scheme, which has a time step 10 times smaller. The use of a TVD partially implicit scheme can greatly enhance the accuracy and efficiency of the saturation update.

3.2. Variable Weighted Schemes

We extend our analysis to the general case where θ is not fixed, but is only constrained by local, not global, stability criteria. This approach is of use in circumstances where the flow speed changes appreciably across the grid and where conventional methods would unnecessarily degrade the accuracy of the solution in slow regions in order to ensure stability in portions of fast flow.

First, we look at (2.30). This will always be obeyed for positive θ and v^{n+1}, and a limiter ϕ in the range described by Eqs. (2.32) and (2.33).

We now investigate (2.29). Again the right-hand limit is always satisfied for values of $\theta \leqslant 1$. We rearrange the left-hand limit of (2.29) to obtain an expression for $\theta_{i+1/2}$:

$$\lambda\theta_{i+1/2}\left(u_i^n + \frac{\phi_{i+1/2}^n}{2r_{i+1/2}^n} v_i^n\right) \geqslant -1 + \lambda v_i^n\left[(1-\theta_{i-1/2})\left(1 - \frac{\phi_{i-1/2}^n}{2}\right) + \frac{\phi_{i+1/2}^n}{2r_{i+1/2}^n}\right] + \lambda u_i^n \theta_{i-1/2}. \tag{3.5}$$

We will now try to construct a scheme for calculating a suitable value for $\theta_{i+1/2}$ which satisfies this TVD property. Note that in Eq. (3.5) $\theta_{i+1/2}$ depends on $\theta_{i-1/2}$ and $\phi_{i-1/2}$ which are calculated at the upstream cell edge. We can simplify this inequality to find $\theta_{i+1/2}$ in terms of parameters that are only measured at the same cell edge by replacing $\theta_{i-1/2}$ and $\phi_{i-1/2}$ with their most restrictive values. We take $\phi_{i-1/2}$ to be zero and obtain

$$\lambda\theta_{i+1/2}\left(u_i^n + \frac{\phi_{i+1/2}^n}{2r_{i+1/2}^n} v_i^n\right) \geqslant -1 + \lambda v_i^n\left(1 + \frac{\phi_{i+1/2}^n}{2r_{i+1/2}^n}\right) + \lambda(u_i^n - v_i^n)\,\theta_{i-1/2} \tag{3.6}$$

which is rearranged to give

$$\theta_{i+1/2} \geqslant 1 - \frac{(1+\lambda(1-\theta_{i-1/2})(u_i^n - v_i^n))}{\lambda(u_i^n + (\phi_{i+1/2}^n/2r_{i+1/2}^n)\,v_i^n)}. \tag{3.7}$$

If $u_i^n \geqslant v_i^n$ the inequality above is always obeyed if we take $\theta_{i-1/2} = 1$ which leaves the simpler expression

$$\theta_{i+1/2} \geqslant 1 - \frac{1}{\lambda(u_i^n + (\phi_{i+1/2}^n/2r_{i+1/2}^n)\,v_i^n)}. \tag{3.8}$$

If $v_i^n > u_i^n$, (3.7) is always satisfied if we take the lowest allowed value of $\theta_{i-1/2}$, which we call $\theta_{\min}$ and we find

$$\theta_{i+1/2} \geqslant 1 - \frac{(1+\lambda(1-\theta_{\min})(u_i^n - v_i^n))}{\lambda(u_i^n + (\phi_{i+1/2}^n/2r_{i+1/2}^n)\,v_i^n)}. \tag{3.9}$$

We can now construct a scheme with a variable value of the weighting parameter θ. The spatial limiter ϕ is calculated as described in the previous section. The Crank–Nicholson parameter θ is allowed to vary from $\theta_{\min} = \frac{1}{2}$, which gives second-order time accuracy, to the totally implicit value of $\theta = 1$ for very large time steps. Thus $\theta_{i+1/2}$ is chosen as

$$\theta_{i+1/2} = \max\left[\frac{1}{2}, 1 - \frac{1}{\lambda(u_i^n + (\phi_{i+1/2}^n/2r_{i+1/2}^n)\,v_i^n)}\right] \tag{3.10}$$

if $u_i^n \geqslant v_i^n$ and

$$\theta_{i+1/2} = \max\left[\frac{1}{2}, 1 - \frac{1-(\lambda/2)(v_i^n - u_i^n)}{\lambda(u_i^n + (\phi_{i+1/2}^n/2r_{i+1/2}^n)\,v_i^n)}\right] \tag{3.11}$$

if $v_i^n > u_i^n$, with similar expressions for $\theta_{i-1/2}$.

Although (3.10) and (3.11) may appear complicated, they are easily coded in practice. All the parameters in the equations are known at the nth time step, except for the time averaged velocity u, (2.26). An estimate of u is made at each Newton iteration.

3.2.1. *Results*

Numerical results are shown in Fig. 11. For CFL numbers of 0.4 and 1, θ was fixed at $\frac{1}{2}$, as in the scheme described

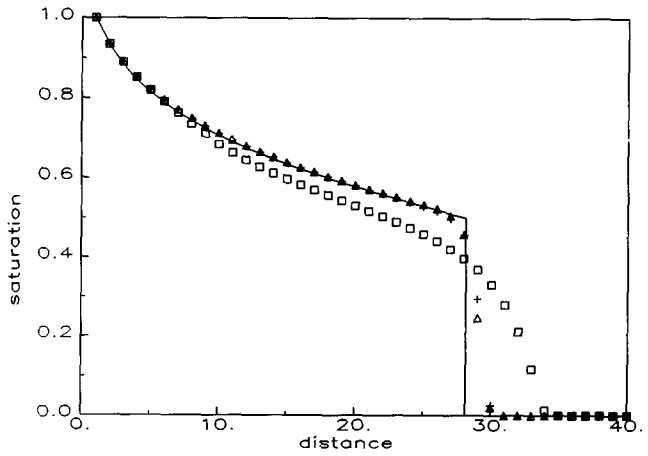

FIG. 11. Solutions with a TVD variably implicit scheme. Squares, CFL number of 4; triangles, CFL = 1; crosses, CFL = 0.4.

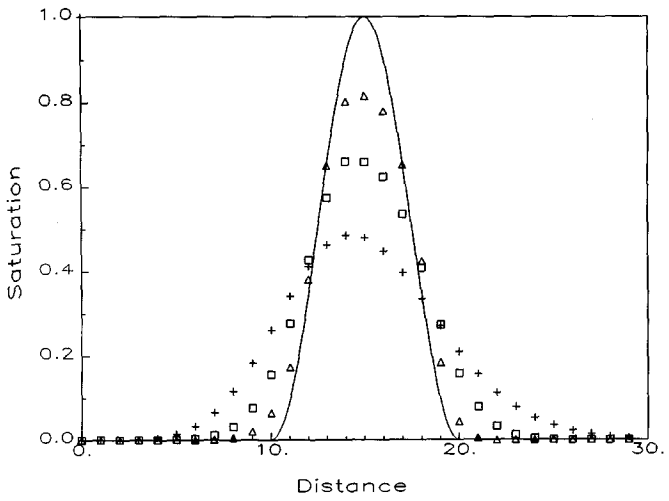

FIG. 12. Linear convection of a $\sin^2$ pulse at a CFL number of 0.4 across one-third of the grid with $N=30$. Crosses, implicit single-point upstream weighting; triangles, partially implicit flux limiting scheme; squares, fully implicit flux limiter.

in Section 3.1. Figure 9 shows the L_1 error norm for a CFL number of 0.4, when $\theta=\frac{1}{2}$—the results are slightly better than for a fully implicit flux limited scheme and comparable with the explicit Sweby method. For a CFL number of 4, the value of θ was larger in regions of fast flow. However, since in this example the shock front moves with almost the maximum wave speed, the resolution of the discontinuity is very similar to that achieved for a fixed value of θ.

Figure 12 shows the numerical solution for the convection of a pulse with a CFL number of 0.4 for a first-order upstream implicit scheme, for a fully implicit flux limiting scheme, and for the partially implicit method with $\theta=\frac{1}{2}$. As we saw with the Buckley–Leverett problem, the first-order implicit methods are more diffusive than their explicit counterparts. However, using $\theta=\frac{1}{2}$ produces results which are very similar to the second-order explicit flux limiting scheme. Figure 13 shows the computed L_1 error norms for $N=30$ to $N=3000$. Using a partially implicit method with $\theta=\frac{1}{2}$ does indeed maintain second-order accuracy.

The real advantage of a partially implicit scheme with a local stability criterion can be demonstrated by a radial flow example, where the flow speed is higher near the injection point, but lower at the advancing front. The region of high flow speed limits an explicit method to extremely small timesteps, while a partially implicit method with θ limited by a global stability criterion would give an over diffuse front. This case is described in the next section.

3.3. A Radial Flow Problem

In this section we present results for a radial Buckley–Leverett flow. If we consider water injected into the centre of a circular region, then (2.1) is replaced by

$$\frac{\partial s}{\partial t}+\frac{1}{r}\frac{\partial}{\partial r}(rf(s,r)), \tag{3.12}$$

where r is the radial distance from the injection centre. Conservation of an incompressible fluid demands that the flux f has the form $f(s,r)=f_w(s)/r$ and, hence, (3.12) reduces to

$$r\frac{\partial s}{\partial t}+\frac{\partial f_w(s)}{\partial r}. \tag{3.13}$$

This is identical to (2.1), except that the saturation s is multiplied by r. We will calculate solutions in a series of annular grid blocks at equally spaced radii r_i. The saturation

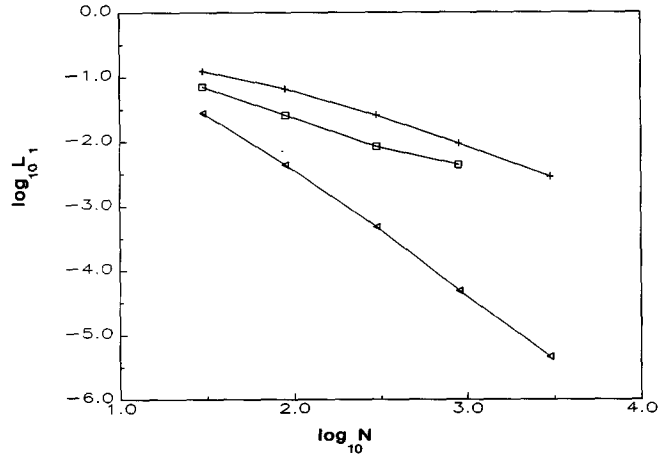

FIG. 13. L_1 error norms; $\log_{10} L_1$ is plotted against $\log_{10} N$ for the linear advection problem shown in Fig. 12. Crosses, implicit single-point upstream weighting; triangles, partially implicit flux limiting scheme; squares, fully implicit flux limiter.

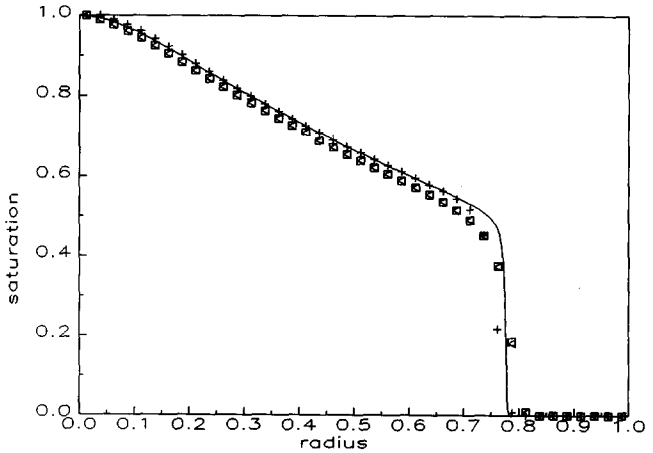

FIG. 14. Solutions for radial flow with $N=40$ and 40 time steps. Squares, totally implicit scheme; triangles, partially implicit with a fixed weighting; crosses, variable weighting.

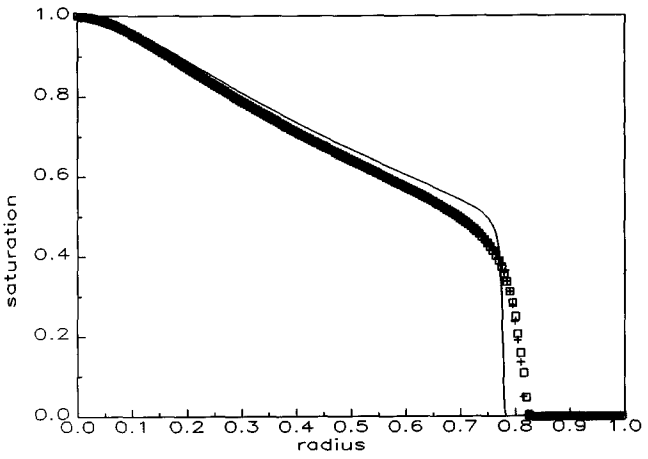

FIG. 15. Solutions for radial flow with $N=200$ and 20 time steps. Squares, totally implicit scheme; crosses, partially implicit with variable weighting.

updates may be calculated using the same schemes that were derived for linear flow except that each increment in the saturation and all the flow velocities are divided by the grid cell radius r_i. We use the same fractional flow $f_w(s)$ as before.

In a radial geometry the local CFL number varies as $1/r$ and hence is very high near the centre of the flow, even when the advancing shock front is at a large radius and has a relatively low speed.

Example results are shown in Fig. 14. A radial Buckley–Leverett flow is solved in 40 grid blocks with 40 time steps. The maximum CFL number in the first grid block is over 35. This means that an explicit scheme would require at least 35 more time steps to ensure stability, which would be hopelessly inefficient. The second-order totally implicit method is stable, but the shock front is poorly resolved. The partially implicit scheme with a fixed weighting θ gives virtually identical results, since the global stability criterion limits θ to approximately 69/70. In a variable weighted scheme a value of θ close to 1 ensures stability near $r=0$, but good temporal and spatial accuracy is maintained near the shock front. Figure 15 shows a more extreme case: a solution with 200 grid blocks and 20 time steps. Here the maximum CFL number is approximately 1764. Even the variable weighted scheme is forced to be almost totally implicit along most of the front and so the results are only slightly superior to the totally implicit scheme.

3.4. A Compressible Flow Example

In this section we present solutions to the compressible one-dimensional two-phase flow problem described in Section 2.4. The flux f is now determined by both the fractional flow and the gradient of a non-trivial pressure distribution. The conserved quantity is now not the fluid volume saturation itself, but the total mass of fluid per unit volume m, where $m=\Phi\rho s$. Φ is the porosity of the medium and ρ is the fluid density, which depends on the pressure.

In this example the treatment is simplified by making the oil and water densities equal. The density is a linear function of pressure and is given by

$$\rho_w=\rho_o=\rho^0+c(p-p_{ref}); \tag{3.14}$$

p_{ref} and ρ^0 are a reference pressure and density, respectively, and c is a small compressibility factor. Equation (2.45) then reduces to

$$\frac{1-s_t}{\Delta t}=-\frac{c(m_o+m_w)}{\Phi\rho^2}\frac{\partial p}{\partial t}+\frac{1}{\Phi\rho}\left(\frac{\partial m_o}{\partial t}+\frac{\partial m_w}{\partial t}\right). \tag{3.15}$$

We then substitute (2.42) and (2.43) into (3.15),

$$\frac{1-s_t}{\Delta t}=-\frac{c(m_o+m_w)}{\Phi\rho^2}\frac{\partial p}{\partial t}+\frac{1}{\Phi\rho}\frac{\partial v_t}{\partial x} \tag{3.16}$$

and, using (2.40),

$$\Phi\rho\left(\frac{1-s_t}{\Delta t}\right)=-c\Phi s_t\frac{\partial p}{\partial t}+\frac{\partial}{\partial x}M\frac{\partial p}{\partial x}. \tag{3.17}$$

This is a parabolic equation which is solved for the pressure field implicitly by backward differencing [26]. M is calculated from the saturation values at the previous time step. We will assume that the fluids are only slightly compressible, so the pressure field does not deviate markedly from the simple form seen in an incompressible flow. Hence a sophisticated high order scheme for solving (3.17) is not necessary. Moreover, this is a paper about hyperbolic conservation equations; the accurate numerical solution of parabolic equations is discussed elsewhere [26].

Once the pressure field is known, the hyperbolic equations (2.42) and (2.43) are solved using the approach of Section 2.4.

We use the following parameters for the results we present below: $p_{ref}=1$ MPa, $c=0.1\ \mathrm{m}^{-2}\mathrm{s}^2$, $\rho_w^0=\rho_o^0=10^6\ \mathrm{Kgm}^{-3}$, $K=0.5$ Darcy, $\phi=0.3$, $\mu_w=1$ cp, $\mu_o=3$ cp, $K_{rw}=s_w^2$ and $K_{ro}=s_o^2$. The fractional flow of water is the same as has been used in the previous examples.

3.4.1. *Results*

In Figs. 16–18 we compare the performance of an implicit first-order upstream weighted scheme with an implicit TVD method and a partially implicit TVD scheme, with a variable θ calculated from (3.10) and (3.11). Results are presented at CFL numbers of 0.42 and 1.5. Both the computed oil and water saturations are plotted—their respective conservation equations are solved separately, but are

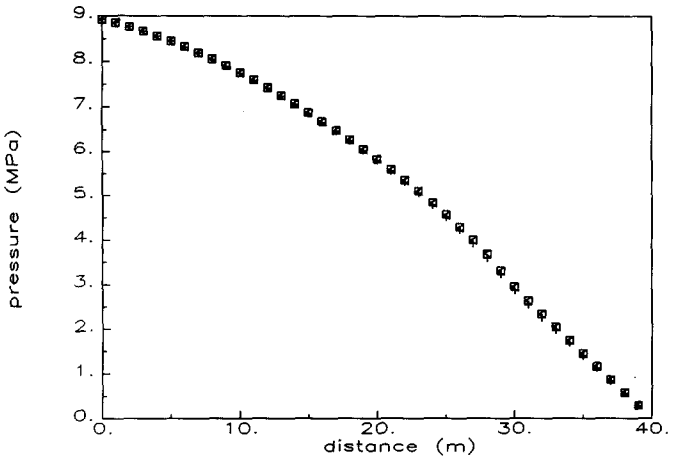

FIG. 16. Pressure profile with a CFL number of 0.42 and $N=40$. Crosses, implicit first-order upstream; squares, implicit TVD method; triangles, variably implicit TVD.

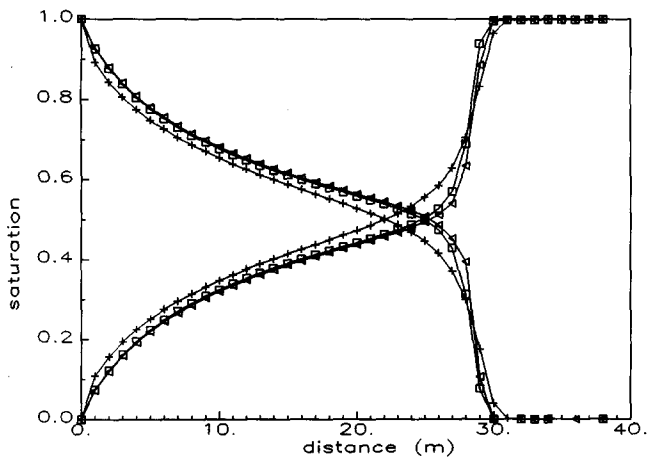

FIG. 17. Compressible flow with a CFL number of 0.42 and $N=40$. Both the oil and water saturation profiles are plotted. Crosses, implicit first-order upstream; squares, implicit TVD method; triangles, variably implicit TVD.

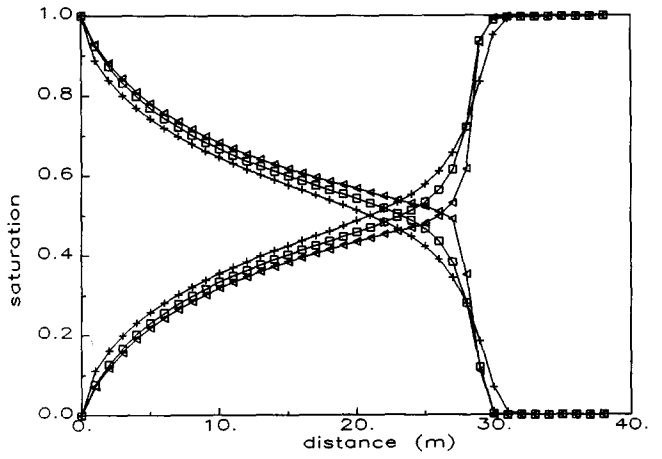

FIG. 18. Compressible flow with a CFL number of 1.5 and $N=40$. Crosses, implicit first-order upstream; squares, implicit TVD method; triangles, variably implicit TVD.

linked together by the mass balance error acting as a source term in the pressure equation (3.17). The solutions resemble the Buckley–Leverett problem discussed earlier, although the fluid compressibility slightly smears the shock front. Figure 17 shows the pressure field for a CFL number of 0.42. Note that, in contrast to the saturation profile, the solution is insensitive to the numerical scheme used. The TVD methods resolve the front better than a simple first-order implicit scheme, and the partially implicit method gives the best results, particularly at the higher CFL number.

3.5. Many Components and Multidimensions

The fully implicit and fully explicit TVD schemes have been implemented in a commercial three-dimensional, multicomponent, three-phase reservoir simulator [27]. Each component conservation law is solved independently along each grid direction. There is no eigencomponent decomposition nor calculation of cross terms. This primitive approach is forced by attempting to build a scheme around a simulator which has already been developed. Nevertheless, the results are extremely encouraging and show considerable improvement over single point upstream weighting which hitherto had been standard in the oil industry. Grid orientation effects are also reduced.

Ideally the extension of these schemes to more complicated situations should be pursued more rigorously. Unfortunately there are no proofs of the TVD property for mixed parabolic/hyperbolic equations, or indeed for systems of hyperbolic equations involving the conservation of three or more components. Also in two and three dimensions the concept of total variation is no longer meaningful. For systems of conservation laws an eigenstate decomposition and update along characteristic directions is recommended, along the lines described for a Godunov scheme by Trangenstein and Bell [3, 24, 25].

We will give a brief indication of how to extend flux limiting schemes to two and three dimensions, although a detailed discussion with numerical examples is beyond the scope of the paper.

In three dimensions the conservation law (2.1) becomes

$$\frac{\partial s}{\partial t}+\nabla\cdot\mathbf{f}=0. \tag{3.18}$$

The vector $\mathbf{f}$, with components (f, g, h) will normally be derived from a fractional flow multiplied by a total velocity or fux. The effective wavespeed $\mathbf{v}(s)$ is also a vector with components $(df/ds, dg/ds, dh/ds)$.

We now find a numerical solution to the equation on a grid labelled by i, j, k coordinates and of spacing $\Delta x, \Delta y, \Delta z$ in the x, y, and z directions. Writing this equation in integral form yields an expression similar to (2.4),

$$s_{ijk}^{n+1} = s_{ijk}^{n} - \lambda_x(F_{i+1/2,j,k} - F_{i-1/2,j,k}) - \lambda_y(G_{i,j+1/2,k} - G_{i,j-1/2,k}) - \lambda_z(H_{i,j,k+1/2} - H_{i,j,k-1/2}), \quad (3.19)$$

where λ_x is $\Delta t/\Delta x$, with similar expressions for λ_y and λ_z, and F, G, and H represent the x, y, and z components of the numerical flux across the grid cell faces, which may be calculated explicitly or implicitly. The components of $\mathbf{v}(s)$ are used to define upstream directions along all three coordinate axes.

A second-order approximation for $F_{i+1/2,j,k}$, is found by Taylor series about a reference state F_{ijk} (if $df/ds \geqslant 0$; $F_{i+1,j,k}$ otherwise),

$$F_{i+1/2,j,k} = F_{ijk} + \frac{\Delta x}{2}\frac{\partial f}{\partial x} + \frac{\Delta t}{2}\frac{\partial f}{\partial t} + \cdots \quad (3.20)$$

from which we obtain

$$F_{i+1/2,j,k} = F_{ijk} + A_{i+1/2,j,k} - \frac{\Delta t}{2}\frac{df}{ds}\left(\frac{\partial g}{\partial y} + \frac{\partial h}{\partial z}\right). \quad (3.21)$$

The final term comes from the approximation to $\partial s/\partial t = -\nabla \cdot \mathbf{f}$ and

$$A_{i+1/2,j,k} = \frac{\Delta x}{2}\frac{\partial f}{\partial x}\left(1 - \frac{df}{ds}\lambda_x\right). \quad (3.22)$$

We approximate the derivatives $\partial f/\partial x$ by $(F_{i+1,j,k} - F_{ijk})/\Delta x$. The y and z derivatives of $\mathbf{f}$ are found by upstream weighting. For example, if dg/ds is greater than zero, then

$$\frac{\partial g}{\partial y} = \frac{g_{i,j,k}^{n} - g_{i,j-1,k}^{n}}{\Delta y}. \quad (3.23)$$

In a totally explicit simulation all the fluxes are evaluated at the nth time level. One approach then is to premultiply $A_{i+1/2,j,k}$ by a limiter $\phi(r_{i+1/2}^{n})$, where

$$r_{i+1/2}^{n} = \frac{A_{i-1/2,j,k}}{A_{i+1/2,j,k}} \quad (3.24)$$

as in (2.6). Separate limiters in the x, y, and z directions for the fluxes F, G, and H, respectively, are found in the same way as in one dimension. The cross-term in (3.21) is not limited. This approach is similar to that described by Bell *et al.* [6] for a Godunov scheme. This scheme is at best

For the partially and fully implicit schemes described before, the time correction in (3.20) was ignored. This leads to a flux of the form

$$F_{i+1/2,j,k} = (1 - \theta_{i+1/2,j,k})\, F_{i+1/2,j,k}^{n} + \theta_{i+1/2,j,k} F_{i+1/2,j,k}^{n+1}, \quad (3.25)$$

where at the n time level,

$$F_{i+1/2,j,k}^{n} = F_{ijk}^{n} + \frac{\phi_{i+1/2,j,k}}{2}(F_{i+1,j,k}^{n} - F_{ijk}^{n}) \quad (3.26)$$

with an analogous expression for the $n+1$ time level. The G and H fluxes are treated similarily with different implicit weightings $\theta_{i,j+1/2,k}$ and $\theta_{i,j,k+1/2}$, respectively. Note that there are no cross terms, so the extension to multiple dimensions is trivial—the calculation of θ and ϕ are performed separately in each of the three coordinate directions. The only complication is that the Jacobian, (2.18), contains two extra non-zero elements per grid block. This method applied as a totally explicit or totally implicit scheme has been successful in two-dimensional simulation [27], and when coupled with a nine-point difference operator to solve the pressure equation, grid orientation effects are considerably reduced. The extensions to a partially implicit scheme which achieves local second-order accuracy by the averaging of the n and $n+1$ time levels will be the subject of further research.

4. CONCLUSIONS

We have presented several numerical schemes for the solution of conservation laws in petroleum reservoir simulation, which are stable regardless of the time step used and are, at best, locally second-order accurate. We developed these schemes by extending the theory of TVD flux limiters to totally and partially implicit schemes.

Compared with first-order schemes these methods offer substantially improved accuracy for no extra cost, particularly where the flow speeds vary across the mesh. In the examples presented here the same accuracy is achieved using one-half to one-quarter the number of time steps, or for the same computational effort, sharp fronts are resolved in fewer than half the number of grid blocks required by a single point upstream weighted method.

The variable weighted scheme is stable for all time steps yet offers a performance comparable to high order explicit methods, which require CFL numbers less than 1. Further

APPENDICES

A.1. Total Variation Diminishing Schemes

In this appendix we define a total variation diminishing scheme and derive TVD criteria for a partially implicit numerical scheme. These results are used in the text to construct suitable TVD schemes. We can only prove these properties for a one-dimensional scalar equation.

We may write a partially implicit scheme for calculating the saturation profile s as

$$s_i^{n+1} - s_i^n = -C_{i-1}^n \Delta s_{i-1}^n + D_i^n \Delta s_i^n - C_{i-1}^{n+1} \Delta s_{i-1}^{n+1} + D_i^{n+1} \Delta s_i^{n+1}, \quad \text{(A1)}$$

where the superscripts refer to the time level and the subscripts refer to the grid cell in which s is evaluated, and we have written

$$\Delta s_{i-1} = s_i - s_{i-1}$$

and

$$\Delta s_i = s_{i+1} - s_i.$$

The coefficients C and D depend on the particular numerical algorithm used.

The total variation, TV, is defined as [28–30]

$$TV^n = \sum_i |\Delta s_i^n|. \quad \text{(A2)}$$

A total variation diminishing or TVD scheme has $TV^{n+1} \leqslant TV^n$. A TVD scheme will converge to the physical solution under certain general conditions [29], but these do not automatically include the partially implicit methods we discuss in the text. Nevertheless, TVD schemes do possess two useful properties, which in the numerical examples we present are sufficient to give reliable and convergent solutions. The first property is that a TVD scheme will not allow unphysical oscillations to develop: a monotonic saturation profile will remain monotonic. Second, a TVD scheme remains bounded, which implies that it is stable.

In the next section we will show the constraints on the coefficients C and D that are necessary for a TVD scheme. Then we will use these constraints to construct a scheme which retains second-order spatial and temporal accuracy in smooth regions of the profile, but which is TVD and thus suppresses the spurious oscillations seen in unstable, or unrestrained second-order methods.

A.2. Criteria for TVD Schemes

First, we rewrite (A1) at grid cell $i+1$, i.e.,

$$s_{i+1}^{n+1} - s_{i+1}^n = -C_i^n \Delta s_i^n + D_{i+1}^n \Delta s_{i+1}^n - C_i^{n+1} \Delta s_i^{n+1} + D_{i+1}^{n+1} \Delta s_{i+1}^{n+1}. \quad \text{(A3)}$$

We then take (A1) from (A3) to obtain

$$\begin{aligned} \Delta s_i^{n+1} - \Delta s_i^n = &- C_i^{n+1} \Delta s_i^{n+1} + C_{i-1}^{n+1} \Delta s_{i-1}^{n+1} \\ &- C_i^n \Delta s_i^n + C_{i-1}^n \Delta s_{i-1}^n \\ &- D_i^{n+1} \Delta s_i^{n+1} + D_{i+1}^{n+1} \Delta s_{i+1}^{n+1} \\ &- D_i^n \Delta s_i^n + D_{i+1}^n \Delta s_{i+1}^n. \end{aligned} \quad \text{(A4)}$$

We rearrange (A4):

$$\begin{aligned} (1 + C_i^{n+1} + D_i^{n+1}) \Delta s_i^{n+1} &= (1 - C_i^n - D_i^n) \Delta s_i^n \\ &+ C_{i-1}^{n+1} \Delta s_{i-1}^{n+1} + C_{i-1}^n \Delta s_{i-1}^n \\ &+ D_{i+1}^{n+1} \Delta s_{i+1}^{n+1} + D_{i+1}^n \Delta s_{i+1}^n. \end{aligned} \quad \text{(A5)}$$

If we impose that $C_i^n \geqslant 0$, $D_i^n \geqslant 0$, $C_i^{n+1} \geqslant 0$, $D_i^{n+1} \geqslant 0$, and $1 \geqslant C_i^n + D_i^n \geqslant 0 \; \forall i$ then all the coefficients in (A5) are positive and we may use the triangle inequality:

$$\begin{aligned} (1 + C_i^{n+1} + D_i^{n+1}) |\Delta s_i^{n+1}| &\leqslant (1 - C_i^n - D_i^n) |\Delta s_i^n| \\ &+ C_{i-1}^{n+1} |\Delta s_{i-1}^{n+1}| + C_{i-1}^n |\Delta s_{i-1}^n| \\ &+ D_{i+1}^{n+1} |\Delta s_{i+1}^{n+1}| + D_{i+1}^n |\Delta s_{i+1}^n|. \end{aligned} \quad \text{(A6)}$$

We now sum both sides of (A6) over all the grid cells i. We note that

$$\sum_i C_i |\Delta s_i| = \sum_i C_{i-1} |\Delta s_{i-1}|$$

with similar relations for D, and thus (A6) gives us

$$\sum_i |\Delta s_i^{n+1}| \leqslant \sum_i |\Delta s_i^n|. \quad \text{(A7)}$$

Hence $TV^{n+1} \leqslant TV^n$.

To conclude, we have shown that a difference scheme written as in (A1) is TVD, provided the coefficients satisfy

$$\begin{aligned} C_i^n &\geqslant 0 \\ D_i^n &\geqslant 0 \\ C_i^{n+1} &\geqslant 0 \\ D_i^{n+1} &\geqslant 0 \\ 1 \geqslant C_i^n + D_i^n &\geqslant 0 \end{aligned} \quad \text{(A8)}$$

for all grid blocks i.

ACKNOWLEDGMENTS

We are grateful to P. K. Sweby, J. J. Barley, and M. G. Edwards for their useful comments on this work. We thank the British Petroleum Company plc for permission to publish this paper.

REFERENCES

1. P. K. Sweby, *SIAM J. Numer. Anal.* **21**, 995 (1984).
2. P. K. Sweby, *Lectures in Applied Math.*, Vol. 22 (Amer. Math. Soc., Providence, RI, 1985), p. 289.
3. J. A. Trangenstein, *Multiphase Flow in Porous Media: Mechanics, Mathematics and Numerics*, Lecture Notes (IBM Scientific Center, Bergen, Norway, 1986).
4. J. A. Trangenstein and J. B. Bell, *SIAM J. Appl. Math.* **49**, 1 (1989).
5. J. B. Bell, P. Colella, and J. A. Trangenstein, *J. Comput. Phys.* **82**, 382 (1989).
6. J. B. Bell, C. N. Dawson, and G. R. Shubin, *J. Comput. Phys.* **74**, 1 (1988).
7. M. A. Christie and D. J. Bond, *SPERE* **2**, 514 (1987).
8. B. Van Leer, *Towards the Ultimate Finite Difference Scheme, I*, Lecture Notes in Physics, Vol. 18 (Springer-Verlag, Berlin, 1973).
9. B. Van Leer, *J. Comput. Phys.* **14**, 361 (1974).
10. B. Van Leer, *J. Comput. Phys.* **23**, 1 (1977).
11. P. K. Sweby and M. J. Baines, *J. Comput. Phys.* **56**, 135 (1985).
12. P. L. Roe, *AMS-SIAM Seminar on Numerical Methods in Fluid Mechanics* (Amer. Math. Soc., Providence, RI, 1985).
13. S. K. Godunov, *Mat. Sb.* **47** (1959); translation by U.S. Dept of Commerce, JPRS 7225 (1960).
14. S. T. Zalesak, *J. Comput. Phys.* **31**, 355 (1979).
15. B. Engquist and S. Osher, *Math. Comput.* **34**, 4575 (1984).
16. R. Courant, K. Friedrichs, and H. Lewy, *Math. Ann.* **100**, 32 (1928).
17. S. R. Chakravarthy and S. O. Osher, in *Proceedings AMS–SIAM Summer Seminar on Large Scale Computations in Fluid Mechanics 1984.*
18. C-E. Forberg, *Introduction to Numerical Analysis* (Addison–Wesley, Reading, MA, 1981).
19. M. V. Wilkes, *A Short Introduction to Numerical Analysis* (Cambridge Univ. Press, Cambridge, UK, 1966).
20. H. C. Yee, *Proc Seminar on Computational Aaerodynamics*, AAA Special Publication, edited by M. Hafez (University of California, Davis, CA, 1986).
21. H. C. Yee, *Computers and Maths with Applications* **12A**, 413 (1986).
22. H. C. Yee, R. F. Warming, and A. Harten, *J. Comput. Phys.* **57**, 327 (1985).
23. B. A. Fryxell, P. R. Woodward, P. Colella, and K. H. Winkler, *J. Comput. Phys.* **63**, 283 (1986).
24. J. A. Trangenstein and J. B. Bell, *SIAM J. Appl. Math.* **49**, 749 (1989).
25. J. A. Trangenstein and J. B. Bell, *SIAM J. Sci. Stat. Comput.* **10**, 817 (1989).
26. G. D. Smith, *Numerical Solution of Partial Differential Equations: Finite Difference Methods* (Clarendon Press, Oxford, 1985).
27. B. Rubin and M. J. Blunt, SPE 21222, presented at the *11th SPE Symposium on Reservoir Simulation, Anaheim, CA, Feb. 17–20, 1991.*
28. P. D. Lax, *Hyperbolic Conservation Laws and the Mathematical Theory of Shock-Waves*, SIAM Regional Conference Series, Lectures in Applied Maths II (SIAM, Philadelphia, 1972).
29. A. Harten, *J. Comput. Phys.* **49**, 357 (1983).
30. A. Harten, *SIAM J. Numer. Anal.* **21**, 1 (1984).